10618–10629 *Nucleic Acids Research, 2021, Vol. 49, No. 18* *Published online 16 September 2021*
https://doi.org/10.1093/nar/gkab769

Identification of host tRNAs preferentially recognized by the *Plasmodium* surface protein tRip

Marta Cela[1], Anne Théobald-Dietrich[1], Joëlle Rudinger-Thirion[1], Philippe Wolff[1], Renaud Geslain[2,*] and Magali Frugier[1,*]

[1]Université de Strasbourg, CNRS, Architecture et Réactivité de l'ARN, UPR 9002, F-67000 Strasbourg, France and [2]Laboratory of tRNA Biology, Department of Biology, College of Charleston, Charleston, SC, USA

Received May 28, 2021; Revised August 17, 2021; Editorial Decision August 21, 2021; Accepted August 26, 2021

ABSTRACT

Malaria is a life-threatening and devastating parasitic disease. Our previous work showed that parasite development requires the import of exogenous transfer RNAs (tRNAs), which represents a novel and unique form of host–pathogen interaction, as well as a potentially druggable target. This import is mediated by tRip (tRNA import protein), a membrane protein located on the parasite surface. tRip displays an extracellular domain homologous to the well-characterized OB-fold tRNA-binding domain, a structural motif known to indiscriminately interact with tRNAs. We used MIST (Microarray Identification of Shifted tRNAs), a previously established *in vitro* approach, to systematically assess the specificity of complexes between native *Homo sapiens* tRNAs and recombinant *Plasmodium falciparum* tRip. We demonstrate that tRip unexpectedly binds to host tRNAs with a wide range of affinities, suggesting that only a small subset of human tRNAs is preferentially imported into the parasite. In particular, we show with *in vitro* transcribed constructs that tRip does not bind specific tRNAs solely based on their primary sequence, hinting that post-transcriptional modifications modulate the formation of our host/parasite molecular complex. Finally, we discuss the potential utilization of the most efficient tRip ligands for the translation of the parasite's genetic information.

INTRODUCTION

Malaria is a common, sometimes fatal, disease known to cause seizures, as well as damage to the brain and other organs. In 2018, there were 228 million cases of malaria reported with an estimated 405 000 deaths worldwide. Children under the age of five are particularly susceptible to infection, with 272 000 deaths reported in a single year (1). All protozoan parasites that cause malaria belong to the genus *Plasmodium* and have a complex life cycle (2). They develop in two different hosts: a common invertebrate (the female *Anopheles* mosquito) and a vertebrate specific for each *Plasmodium* species. Over 250 *Plasmodium* species infect reptiles, birds, and mammals. Among them, six species infect humans including *Plasmodium falciparum,* the most dangerous strain, especially for children (3).

We have previously shown that sporozoites (i.e. the extracellular infective form of *Plasmodium* isolated from salivary glands of infected mosquitoes) import extracellular transfer RNAs (tRNAs) *via* a surface protein that we named tRip for tRNA import protein (4). tRNAs are small noncoding ribonucleic acids that are essential for the translation of messenger RNAs. They are first aminoacylated by cognate aminoacyl-tRNA synthetase (aaRSs), then they transport their amino acid to the ribosome for the polymerization of cellular proteins (5). tRip is expressed over the entire parasite life cycle; *in vitro,* its specific and strong affinity for tRNAs relies on interactions between its C-terminal domain with the three-dimensional structure of tRNAs. Immunolocalization and cell fractionation experiments demonstrated that tRip is an integral plasma membrane protein (at both the sporozoite and blood stages) that displays its C-terminal tRNA-binding domain into the extracellular space. Further experiments with a tRip knock-out parasite showed that although the protein is not essential for survival, it is important for overall parasite fitness and required for the import of extracellular tRNAs (4).

Plasmodium tRip was bioinformatically identified when searching for homologs of well-known tRNA-binding modules such as *Aquifex aeolicus* Trbp111 (6,7) and *Saccharomyces cerevisiae* Arc1p (8). tRip is highly conserved amongst *Plasmodia* (Figure 1A), and it displays an N-terminal GST-like domain and a C-terminal OB-fold tRNA-binding domain. OB-folds are often fused to the N- or C-termini of aaRSs and increases their affinities for cognate tRNAs and are found in all kingdoms of life (9). OB-fold tRNA-binding domains can also be free-standing or fused to non-catalytic proteins. For example, *Aquifex*

*To whom correspondence should be addressed. Tel: +33 388417109; Email: m.frugier@ibmc-cnrs.unistra.fr
Correspondence may also be addressed to Renaud Geslain. Tel: +1 843 953 8080; Email: geslainr@cofc.edu

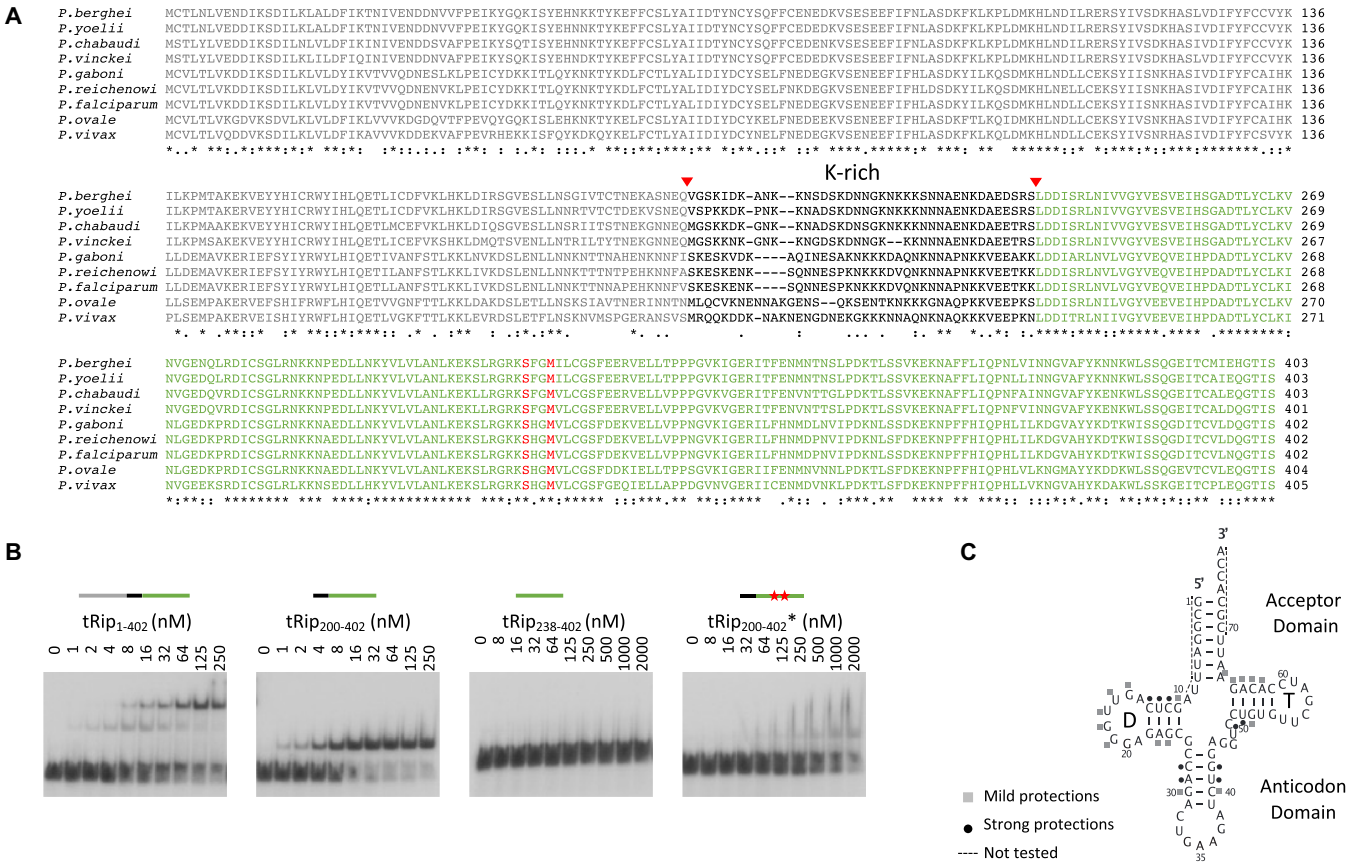

Figure 1. Characterization of tRNA:tRip recognition. (**A**) Alignments of *Plasmodium* tRip homologs. The amino acid sequences of tRip homologs were retrieved from the eukaryotic pathogens database (50). Sequences reveal a three-part organization: (i) an N-terminal GST-like domain (grey), (ii) a short polypeptide rich in lysine residues (black), and (iii) a conserved C-terminal tRNA-binding domain (green). Red arrowheads indicate the N-terminal extremities of $tRip_{200\text{-}402}$ and $tRip_{238\text{-}402}$, two tRip variants with truncated N-termini. Residues S_{312} and M_{315} are mutated into alanine in $tRip_{200\text{-}402}$* are indicated in red. (**B**) tRNA binding capabilities of recombinant tRip variants. EMSAs were performed with a constant concentration of radiolabeled $Sctr^{Phe}_{GAA}$ and increasing concentrations of $tRip_{1\text{-}402}$, $tRip_{200\text{-}402}$, $tRip_{238\text{-}402}$ and $tRip_{200\text{-}402}$*. Concentrations and schematized tRip domains are indicated on top of each gel, with the same color code as described above. (**C**) Summary of Pb^{2+} acetate footprint. Nucleotides protected from lead cleavage are displayed on the cloverleaf representation of $Sctr^{Phe}_{GAA}$. Black spheres and grey squares indicate nucleotides strongly and mildly protected respectively. Dotted lines at the 5′ and 3′ ends highlight non-tested tRNA nucleotides.

aeolicus Trbp111 is a free-standing homodimeric OB-fold that binds to all tRNAs with high affinity ($K_d = 32$ nM) sequence independently based on the recognition of the conserved 'tRNA elbow' structure (6).

The eukaryotic homolog of Trbp111 is a monomeric OB-fold. Monomeric OB-folds display additional positively charged residues at their N-terminus and a C-terminal portion that coincides to the bacterial Trbp homodimer dyad axis (10,11). Eukaryotic proteins containing tRNA-binding modules are essential for assembly of multi-aaRSs (MARS) complexes and prevent tRNA diffusion in the cytoplasm; tRNA channeling to MARS directly improves the efficiency of tRNA aminoacylation which in turns enhances translation (8,12,13). In *Homo sapiens*, an OB-fold called EMAPII (Endothelial Monocyte-activating Polypeptide II), is involved in cell signaling when cleaved from AIMP1 or cytosolic tyrosyl-tRNA synthetase (14,15,16).

Although tRNA-binding modules have been one of the foci of our scientific community, it should be noted that only two of them have been investigated so far for their specificity toward individual tRNA species, namely *S. cerevisiae* Arc1p and *Trypanosoma brucei* MCP2 (17,18). *S. cerevisiae* Arc1p has a GST-like N-terminal domain involved in the formation of the small yeast MARS complex by binding to the N-terminal domains of both glutamyl- and methionyl-tRNA synthetases (ERS and MRS, respectively) (8,19); the corresponding ternary complex regulates the cellular localization of MRS and ERS (20,21). Within the complex, the C-terminal OB-fold domain specifically increases the affinity of MRS and ERS for their cognate tRNA substrates, namely $tRNA^{Met}$ and $tRNA^{Glu}$ respectively (22). Interestingly, free-standing Arc1p exhibits broader specificity toward tRNA species (18). Likewise, free-standing *T. brucei* MCP2, a tRNA-binding protein that normally associates with the parasite MARS-complex, displays new patterns of affinities and specificities toward tRNAs including species that are not substrates of the subset of aaRSs present in MARS (17). Arc1p- and MCP2-associated tRNAs do not share any obvious features and the experimental procedures employed did not allow a systematic assessment of individual tRNA species. The bottom line is that the molecular rules that govern the formation of these RNA/protein com-

plexes remain largely unknown for all OB-fold RNA binding proteins.

Based on our earlier electrophoretic mobility shift assays (EMSAs), we reported that tRip forms complexes with all human tRNAs when present in non-limiting concentrations (4). In the present study, we revisited this observation to systematically assess the selectivity of *P. falciparum* tRip toward each human tRNA. We employed a proven technique, where tRip-bound tRNAs isolated from total human tRNA extracts were hybridized on tRNA microarrays for efficient identification. This approach named MIST for Microarray Identification of Shifted tRNA, was first used to identify non-cognate tRNAs complexed to yeast arginyl-tRNA synthetase (RRS) (23). Since the tRNA binding domain of tRip is located on the parasite surface away from the cytoplasmic content, its binding specificity was tested exclusively against total tRNAs from its human host in the absence of any parasite tRNAs or other molecules. The overarching objective of this study was to clarify how tRip interacts with human tRNAs and to determine which tRNAs are most likely to enter the parasite, to give us valuable insight into the role of these imported species in the physiology of *Plasmodium*.

MATERIALS AND METHODS

tRip cloning and production

Plasmodium falciparum wild-type and variant tRip genes (1–402, 200–402, 238–402 and 200–402*) were cloned into the expression vector pET15b to produce proteins fused to a 6-histidine tag at their N-termini. The asterisk in $tRip_{200\text{-}402}$* indicates Ser312Ala/Met315Ala double mutant. Expression was induced with 0.5 mM isopropyl-β-D-thiogalactopyranoside at 18°C overnight and His_6-tagged proteins were purified on Ni-NTA resin (Sigma-Aldrich). Purifications were performed in the presence of 50 mM HEPES–NaOH pH 8.0, 300 mM NaCl, 5 mM β-mercaptoethanol, 10% (v/v) glycerol, and 0.005% (w/v) *n*-dodecyl-β-D-maltopyranoside (DDM). The wash step recommended by the manufacturer was modified to include a linear and increasing gradient of NaCl from 300 mM to 2 M followed by a decreasing gradient back to 300 mM NaCl to remove any nucleic acids interacting with the resin-bound tRip. Recombinant proteins were further purified by gel filtration (Superdex 200, GE Healthcare) in 25 mM HEPES–KOH pH 7.0, 75 mM KCl, 5 mM β-mercaptoethanol, 10% (v/v) glycerol and 0.005% (w/v) DDM, then dialyzed overnight at 4°C against the same buffer containing 30% (v/v) glycerol and finally stored at −80°C.

RNA preparation

HeLa cells were washed in phosphate-buffered sodium (PBS) and total RNA was extracted using Tri-Reagent (Sigma-Aldrich) according to the manufacturer's instructions. Further fractionation was performed on a gel filtration column (Superdex 200) in 50 mM HEPES−KOH pH 7.5, 150 mM NaCl in order to isolate tRNAs from mRNAs and ribosomal RNAs. Human $tRNA^{Arg}_{ICG}$ was purified by hybridization to a complementary 3′-biotinylated probe (5′-ATCCGTAGTCAGACGCGTTA-TCCATTGC-3′) as described previously (24). *Saccharomyces cerevisiae* native tRNAs ($tRNA^{Trp}_{CCA}$, $tRNA^{Leu}_{CAA}$, $tRNA^{Val}_{AAC}$, $tRNA^{Asp}_{GTC}$, $tRNA^{Met}$i, $tRNA^{Phe}_{GAA}$ and $tRNA^{Ile}_{IAU}$) were purified as in (25,26) and their sequences were confirmed by mass spectrometry (27). The genes coding four human tRNAs ($tRNA^{Thr}_{CGT\text{-}2}$, $tRNA^{Leu}_{TAG}$, $tRNA^{Asp}_{GTC}$ and $tRNA^{Asn}_{GTT}$) and *S. cerevisiae* $tRNA^{Phe}_{GAA}$ were cloned under the control of the T_7 RNA polymerase promoter to produce the corresponding transcripts *H. sapiens* (Hs) and *S. cerevisiae* (Sc) tRNA ($Hstr^{Thr}_{CGT\text{-}2}$, $Hstr^{Leu}_{TAG}$, $Hstr^{Asp}_{GTC}$, $Hstr^{Asn}_{GTT}$ and $Sctr^{Phe}_{GAA}$). In addition, a $minihelix^{Phe}$ was also synthesized. Transcriptions were performed for 3 h at 37°C with 100 ng/μl of linearized plasmid and 5 ng/μl of T_7 RNA polymerase in 40 mM Tris−HCl pH 8.1, 10 mM dithioerythritol (DTE), 2 mM spermidine, 11 mM $MgCl_2$ and 4 mM of GMP, ATP, CTP, GTP and UTP. Transcripts were purified on a 12% denaturing polyacrylamide gel (19:1, 8 M urea), electroeluted, and precipitated. Their concentrations were determined by UV absorbance at 260 nm.

Radioactive labeling of the 3′ end of tRNAs ($Sctr^{Phe}_{GAA}$ and tRNAs used with MIST) was performed on 140 pmoles of tRNA/transcript with 20 μCi [α^{32}P]ATP in 50 mM Tris−HCl pH 8.0, 50 μM CTP, 10 mM $MgCl_2$, 8 mM DTE, and 6 ng/μl of yeast tRNA nucleotidyltransferase for 30 min at 37°C (28). Minihelices were 5′ radiolabeled as described in (29). Non-incorporated radioactive nucleotides were removed on a NAP-5 column (GE Healthcare, Buckinghamshire, UK) before EMSAs and MIST experiments or on a 12% denaturing polyacrylamide gel prior to footprinting experiments.

Electrophoretic mobility shift assays (EMSAs)

Prior to use, all tRNAs and transcripts were renatured in H_2O by heating at 65°C for 2 min followed by cooling for 10 min at room temperature in the presence of 10 mM $MgCl_2$. For direct EMSAs, radiolabeled RNAs (1000 cpm/μl) were incubated for 20 min on ice in 25 mM HEPES–KOH pH 7.0, 5 mM $MgCl_2$, 75 mM KCl, 10% (v/v) glycerol, 20 nM oligo-dT with increasing concentrations of tRip monomer: 0 to 250 nM $tRip_{1\text{-}402}$ and $tRip_{200\text{-}402}$ or 0 to 2000 nM $tRip_{238\text{-}402}$ and $tRip_{200\text{-}402}$*. For competitive EMSAs, radiolabeled $Sctr^{Phe}_{GAA}$ (1000 cpm/μl) and 30 nM $tRip_{1–402}$ monomers were incubated in the presence of increasing amounts of unlabeled RNA competitors (12.5, 25, 50 and 100 nM). tRNA:tRip complexes were separated on a 6% native polyacrylamide gel (37.5:1) in TBE buffer (Tris/Borate/EDTA) at 140V for 90 min at 4°C. Gels were dried and radioactive signals were quantified by phosphorimaging on a Typhoon™ FLA 7000 (GE Healthcare). The ratio Free $Sctr^{Phe}_{GAA}$/(Free + Bound $Sctr^{Phe}_{GAA}$) was plotted versus the concentration of competitive transcripts. The slope values were used to determine the dissociation rate (K_d) for each tRNA:tRip complex to assess their relative affinities for tRip. Molecules were tested at least three times; the mean of the slopes and SEM.

Footprint

$tRip_{200\text{-}402}$ was previously dialyzed against 10 mM HEPES–NaOH pH 7.4, 10 mM NaCl, 10 mM $MgCl_2$. One μM

$Sctr^{Phe}_{GAA}$ (5000 cpm/μl) was incubated in Lead Buffer (50 mM Tris-acetate pH 7.5, 5 mM magnesium acetate, 50 mM potassium acetate) with increasing concentrations of protein (2.6, 5.2 and 7.8 μM) for 20 min on ice to allow complex formation. Freshly prepared lead acetate solution (50 mM) was added to each sample to a final concentration of 5 mM and cleavage reactions were run at 25°C for 8 min, quenched by adding EDTA (33 mM), extracted with phenol, and ethanol precipitated (in the presence of 0.1 μg/μl of glycogen). The pellets were washed twice with 70% EtOH, vacuum-dried, dissolved in gel loading buffer (90% formamide, 0.5% EDTA, 0.1% xylene cyanol and 0.1% bromophenol blue), heated for 2 min at 90°C, and analyzed on a 12% (19:1) denaturing polyacrylamide gel. A lead-free control was run in parallel. For nucleotide assignment, alkaline degradation was performed for 4 min at 80°C in 50 mM $NaHCO_3$ pH 9.0 and the G ladder was obtained by iodine cleavage of the $Sctr^{Phe}_{GAA}$ containing at most one phosphorothioate G per molecule (30).

MIST

Increasing amounts of total tRNA (8, 20 and 40 μM), purified from HeLa cells, were incubated for 20 min at 4 ºC with 2 μM tRip dimers in a total volume of 100 μl with EMSA buffer. These mixtures were loaded on a 6% native gel and separated for 4 h at 140 V (10 ºC). Bands were visualized by UV shadowing and tRNAs were gel extracted using the crush & soak method (300 mM sodium acetate, 1 mM EDTA, 0.1% SDS) (31). The tRNAs were 3′-radiolabeled as described above before being hybridized onto human tRNA arrays. Each chip consisted of 48 different probes, repeated eight times (for a complete and generic protocol please refer to (32)). These probes hybridize either to a unique tRNA species (Arg-3h, Asn-1h, Asp-1h, Gly-2h, His-1h, Leu-3h, Lys-1h, Lys-3h, Lys4H, Met-1h, Sec-1h, Thr-3h, Thr-4h, Val-4h), a group of tRNA isodecoders (Arg-1h, Arg-4h, Glu-2h, Ile-2h, Leu-2hn, Leu-4h, Leu-6h, Lys-2h, Met-2h, Phe-1h, Ser-1h, Ser-3h, Thr-1h, Thr-2h, Thr-5h, Tyr-2h), several isoacceptors specific to the same amino acid (Ala-2h, Arg-2h, Glu-1h, Gly-1h, Leu-1h, Pro-1h, Ser-2h, Val-1h), or tRNAs specific to different amino acids (Glu-3h, Ser-4h, Thr6h, Tyr-1h, Val-3h) (Supplementary Figure S1). The tRNA arrays were hybridized and washed in an automated microarray hybridizer as described in (32). The radioactive signal at each spot was captured by phosphorimaging, quantified using ImageJ upgraded with a microarray plugin, and processed in Excel spreadsheets. Data were normalized by calculating the ratio: Bound tRNA/(bound tRNA + free tRNA).

RESULTS

Topology of tRNA:tRip complexes

Figure 1A shows an alignment of *P. falciparum* tRip with eight representative sequences from other *Plasmodia*. A high degree of similarity is evident in both the N- (GST-like) and C-terminal (EMAPII-like) domains whereas the short lysine-rich domain (K-rich) varies significantly. Recombinant *P. falciparum* tRip variants were expressed in *Escherichia coli* from pET15b plasmids fused to an N-terminal His-tag. Both $tRip_{200\text{-}402}$ and $tRip_{238\text{-}402}$ were derived from the C-terminal OB-fold structure, with or without the K-rich domain, respectively. Based on the crystal structure of the bacterial Trbp111 and the model built with interacting tRNA, 15 amino acids were identified as potential candidates for tRNA recognition; mutagenesis experiments have shown that substitutions of two of these amino acids, serine 82 and methionine 85, had a significant effect on Trbp111′s ability to bind tRNA (7). These two residues are conserved in *P. falciparum* tRip where they correspond to Ser_{312} and Met_{315} (Figure 1A). Therefore, we substituted them simultaneously with alanine and checked the ability of the corresponding mutant protein, $tRip_{200\text{-}402}$* (asterisk indicates double mutant), to bind tRNAs.

Recombinant $tRip_{1\text{-}402}$ and $tRip_{200\text{-}402}$ bind to *S. cerevisiae* $tRNA^{Phe}_{GAA}$ transcript ($Sctr^{Phe}_{GAA}$) with comparable apparent dissociation constants (K_d = 25.9 (±7.1) and 13.6 (±1.6) nM, respectively), as determined by EMSA (Figure 1B). In contrast, $tRip_{238\text{-}402}$ and the mutated $tRip_{200\text{-}402}$* displayed very weak tRNA binding capabilities, with K_d values higher than 2 μM, confirming that the K-rich sequence and the conserved Ser_{312} and Met_{315} act synergistically for efficient tRNA binding.

Previous footprint experiments (4) with fully-modified, native *S. cerevisiae* $tRNA^{Asp}_{GTC}$ showed that only a few positions were protected, presumably because of limited access by the bulky nucleases, even in the absence of tRip. We repeated the footprint experiments on $Sctr^{Phe}_{GAA}$ using lead (Pb^{2+}) as a probing agent. The absence of post-transcriptional modifications and the use of a small chemical specific to single-stranded regions (33) allowed us to probe nearly the entire tRNA sequence and determine more precisely the regions recognized by $tRip_{200\text{-}402}$ (Figures 1C and Supplementary Figure S2). Upon complex formation, both the anticodon- and D-arms were strongly protected from cleavage, whereas moderate protections were observed in the D-loop and the T-arm. Notice that there is almost no hydrolytic cleavage in $Sctr^{Phe}_{GAA}$ alone (control lane without Pb^{2+} or tRip) confirming that this tRNA was properly folded and stable. This tRNA-binding pattern is reminiscent of that observed with Trbp111 (34), as both tRip and Trbp111 bind to the corner of the L-shaped tRNA.

Stoichiometry and oligomeric organization of tRNA:tRip complexes

To determine the stoichiometry of the tRNA:tRip complex, recombinant $tRip_{1\text{-}402}$ was incubated with increasing concentrations of $Sctr^{Phe}_{GAA}$ and complex formation was analyzed on a native gel (Figure 2A). Seven tRNA:tRip ratios were tested ranging from 0.19:1 to 1.5:1. As expected, tRip tends to multimerize when the tRNA concentration is limiting in the sample, a trend that was previously observed with Arc1p (18). Conditions that include at least two tRip proteins per tRNA molecule are sufficient to shift the entire tRNA population. Decreasing the protein to tRNA ratio yields increasing proportions of free-standing tRNA. A Scatchard plot further confirmed that tRip is saturated at a tRNA:tRip ratio of 1:2 (Figure 2B). However, since the biologically relevant oligomeric organization of tRip is an

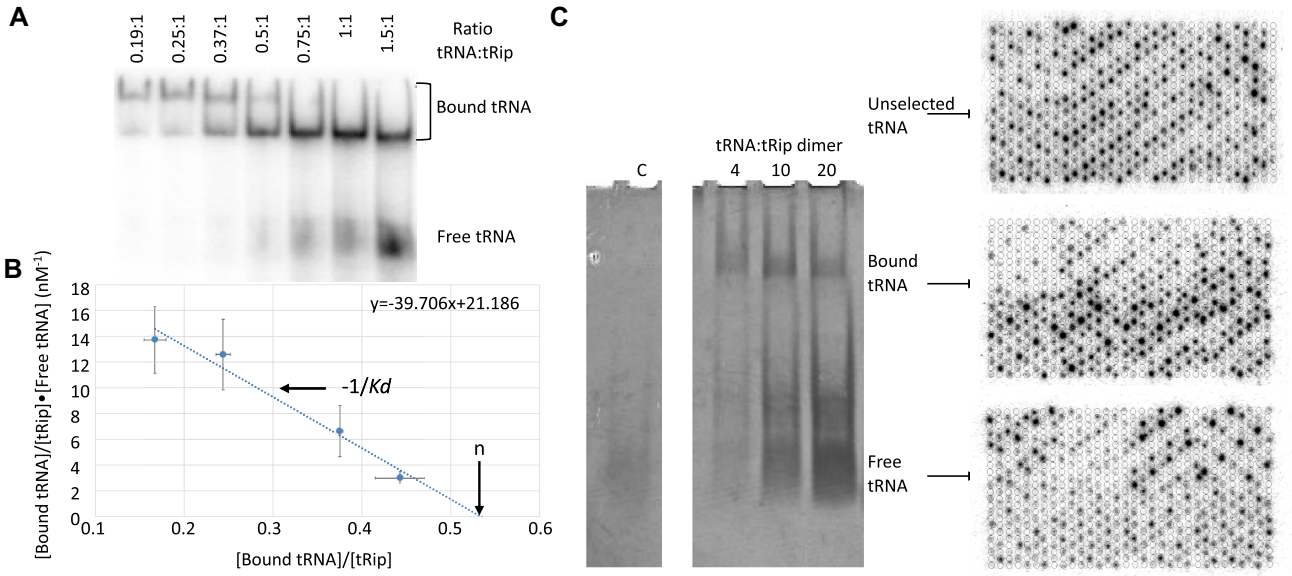

Figure 2. Establishment of biologically relevant conditions for MIST. (**A**) Determination of the stoichiometry in the tRNA:tRip complex. EMSAs were conducted in the presence of 2 μM tRip monomers and increasing concentrations of radiolabeled $Sctr^{Phe}_{GAA}$ to establish seven tRNA:tRip monomer ratios: 0.19:1; 0.25:1; 0.37:1; 0.5:1; 0.75:1; 1:1 and 1.5:1. Gel images are representative of 3 biological replicates. (**B**) Scatchard representation. The 3 independent replicates were quantified and averaged. The concentrations of bound tRNAs [bound tRNA], free tRNA [free tRNA] and tRip [tRip] were used to plot [Bound tRNA]/([tRip]•[Free tRNA]) *versus* [Bound tRNA]/[tRip]. The corresponding graph was used to extrapolate (i) the number of tRNA-binding sites per protein molecule (mean ± SEM = 0.53 ± 0.07) from the intersection of the trendline and the x-axis and (ii) the K_d (mean ± SEM = 28.5 ± 5.2 nM) from the slope which equates to $-1/K_d$. (**C**) Selection and analysis of MIST experiments. tRNA:tRip complexes were separated from free tRNAs on 6% native gel and visualized by UV shadowing. The concentration of tRip dimers remained constant (2 μM), while the concentration of human total tRNA varied (8, 20 and 40 μM). The control lane contains 2 μM tRNA in the absence of tRip. tRNAs were eluted from the gel and radiolabeled. Three examples of hybridized tRNA arrays are shown; they correspond to *H. sapiens* crude tRNA (Unselected) as well as the bound and free tRNA of the four tRNAs per tRip dimer condition. Our in-house array-manufacturing platform allows printing of up to 768 spots per glass slide. To prevent signal overlapping between consecutive spots and allow for proper background subtraction, we only printed 383 spots while still using the whole printing area. In other words, arrays were prepared by skipping every other spot.

α_2 homodimer (4,35), the stoichiometry in the tRNA:tRip dimer complex can be considered to be 1:1.

Systematic assessment of tRip specificity with tRNA microarrays

MIST (Microarray Identification of Shifted tRNAs) was designed to identify tRNAs in a population based on their affinity for a given protein (23). This approach was adapted from a fluorescent microarray method developed in the Pan laboratory (36), which allows the quantification of cellular tRNAs in total tRNA extracts, and relies on microarrays printed with DNA oligonucleotides complementary to full-length tRNA sequences (Supplementary Figure S1). The longer length of these tRNA probes significantly increases their hybridization efficiency and allows them to distinguish between tRNAs that differ by as few as eight nucleotides (36). MIST was designed around the same established probes and proven protocol. However, MIST differs notably from the original method in that (i) the tRNAs investigated are radioactively labeled, a treatment that does not alter any tRNA functionalities especially their interaction with molecular partners; (ii) a selection step is added before hybridization onto microarrays, which consists of isolating tRNA:protein complexes (bound tRNAs) from free tRNAs via native gel electrophoresis and (iii) the proportion of each tRNA in the sample is determined by the intensity of the radioactivity retained at each spot on the chip.

Complex formation. To establish the proper experimental conditions for MIST we reasoned that: (i) tRNAs should be in excess to favor competition and allow tRip to naturally select the best interactants from crude human tRNAs and (ii) one tRNA molecule is the strict minimum required to saturate one dimeric $tRip_{1-402}$ *in vitro* (Figure 2A and B). Accordingly, different tRNA:tRip ratios were used. While the protein concentration remained constant (2 μM dimer), the amount of tRNA was set to 8, 20 and 40 μM, which corresponds to 4, 10 and 20 times more total tRNAs than tRip dimers. Figure 2C shows the result of a native purification gel. tRNAs present in the complex and the free fraction were recovered from the gel and analyzed with tRNA microarrays for all three experimental conditions. As control experiments, two unselected samples of crude tRNAs purified from HeLa cells (unselected tRNA-1 and unselected tRNA-2) were also analyzed.

Hybridization of complexed tRNAs on tRNA microarrays. Figure 2C shows three examples of hybridized microarrays used to determine the proportion of each tRNA in unselected, tRip-bound, and free tRNA fractions (in the ratio

of four tRNAs per tRip dimer). The obvious variations in spot patterns indicate that the proportions of individual tRNAs in our three samples vary significantly depending on the conditions used in each case.

Analysis of tRNA microarrays. Microarrays were quantified with ImageJ and intensities were averaged for the 8 replicates of each probe as described previously (23,32). Raw results are shown in Supplementary Figure S3A–E and summarized in Figure 3. Four tRNAs namely $tRNA^{Ile}_{rAT}$, $tRNA^{Cys}_{GCA}$, $tRNA^{Gln}_{yTG}$ and $tRNA^{Trp}_{CCA}$ were not observed, presumably because their concentrations fall below our detection threshold.

Control experiments where crude tRNA from HeLa cells were hybridized on two different arrays (unselected tRNAs-1 and unselected tRNAs-2) show comparable results to each other, confirming that the experimental procedure is reproducible (Supplementary Figure S3A and B). Moreover, as expected, the average of unselected tRNAs-1 and unselected tRNAs-2 (**U**, average of unselected tRNAs) matches the average of the 'bound + Free' tRNAs after selection (**S**, average of selected tRNAs) (Supplementary Figure S3A). Some species, including $tRNA^{Asp}_{GTC}$, $tRNA^{Sec}_{TCA}$ $tRNA^{Thr}_{CGT-2}$, $tRNA^{Arg}_{ICG}$, $tRNA^{Lys}_{TTT-1}$, $tRNA^{Arg}_{TCT}$, and $tRNA^{Ile}_{TAT}$, show contrasting distributions between the bound and free fractions (Supplementary Figure S3A) as anticipated, illustrating that tRNAs that form complexes with tRip are logically displaced from the population of free-standing tRNAs and confirming the utility of this method.

We used the ratio of (bound tRNAs)/(bound + free tRNAs) (Figure 3) as a proxy for the likelihood of a given tRNA to form a complex with tRip. tRNAs showing above average (>0.5) binding capacities are highlighted with shades of orange whereas below average species (<0.5) are highlighted with shades of blue. We would like to emphasize that the ranking of the tRNAs is independent of their concentrations in the initial sample (column MIST, based on the average of three experiments), indicating that the selectivity of complex formation is based on tRNA features other than their mere abundance (Figure 3, compare MIST and U). Overall, our results clearly show that tRip does not recognize all tRNAs equally since certain tRNAs are enriched and others are depleted after selection: tRNAs binding most effectively to tRip correspond to $tRNA^{Leu}_{CAG}$, $tRNA^{Val}_{TAC}$, $tRNA^{Ala}_{hGC}$, $tRNA^{Asn}_{GTT}$, $tRNA^{Ser}_{AGA}$ and $tRNA^{Leu}_{wAG}$, whereas tRNAs with the lowest affinities for tRip include $tRNA^{Ala}_{IGC}$, $tRNA^{Ser}_{CGA}$, $tRNA^{Thr}_{CGT-2}$, $tRNA^{Asp}_{GTC}$, $tRNA^{Arg}_{ICG}$, $tRNA^{Pro}_{hGG}$, $tRNA^{Thr}_{TGT-1}$ and $tRNA^{Sec}_{TCA}$. Furthermore, the ranking of these specific tRNAs remains globally uniform regardless of the tRNA:tRip ratio in the experiment.

Search for the molecular features supporting tRNA:tRip complex formation

We attempted to purify several *H. sapiens* native tRNAs from HeLa cells to assess their ability to bind to tRip through standard and competitive EMSAs. Native tRNA purifications were performed by hybridization of the target tRNA to a biotinylated probe, followed by retention on streptavidin resin (24). The biotinylated probes were designed to hybridize to their tRNAs between the D-loop and the anticodon loop. Purification yields varied considerably between the different species. To assess their purity, 0.5 μg of each eluate was analyzed by mass spectrometry: $tRNA^{Arg}_{ICG}$ was found to be the only species with suitable purity for affinity studies. As a side note, we would like to emphasize that this quality test allowed us to identify, for the first time, the post-transcriptional modifications present on this tRNA (Supplementary Table S1A). Unfortunately, the amounts recovered were not sufficient to conduct competitive EMSAs. Finally, the analysis of all other samples invariably showed the presence of many contaminants, making them unsuitable for further experimentation.

As an alternative we used several purified native *S. cerevisiae* tRNAs (Figure 4A), which were validated by mass spectrometry to verify their sequence and the presence of expected post-transcriptional modifications (Supplementary Table S1B). They were all tested under competitive conditions: Complexes between tRip and radiolabeled $Sctr^{Phe}_{GAA}$ were pre-formed, followed by the addition of increasing concentrations of competitive unlabeled tRNAs. Competitive tRNAs displace $Sctr^{Phe}_{GAA}$ based on their affinity for tRip (see Figure 4B for representative gels); the higher the affinity for tRip, the greater the dissociation rate of the complex. Each *S. cerevisiae* native tRNA was tested at least 3 times and the mean and standard error of the mean (SEM) were calculated (Figure 4A). EMSA was sensitive enough to quantify tRNA affinities based on the ability of each tRNA to displace the pre-existing complex. We organized the tRNAs into three groups (high, mid, and low) according to their dissociation rates. The K_d values between the high group (represented by $tRNA^{Ile}_{IAT}$/$tRNA^{Val}_{AAC}$) and the low group (represented by $tRNA^{Asp}_{GTC}$/$tRNA^{Phe}_{GAA}$) varied by 2.5-fold and were significant (P-value < 0.05).

Competitive EMSAs were also performed with tRNA transcripts lacking post-transcriptional modifications. We chose to test tRNA transcripts corresponding to weak tRip-binders such as *H. sapiens* $tRNA^{Thr}_{CGT-2}$ and $tRNA^{Asp}_{GTC}$ and strong tRip-binders such as *H. sapiens* $tRNA^{Leu}_{TAG}$ and $tRNA^{Asn}_{GTT}$ (Figure 3, Supplementary Table S2). Dissociation rates between transcripts were not as diverse as those of the native yeast tRNAs, which indicates that stripping tRNAs of all post-transcriptional modifications disrupts their individual binding abilities (Figure 4). This was further illustrated when challenging $Sctr^{Phe}_{GAA}$:$tRip_{1-402}$ complexes with $minihelix^{Phe}$ mimicking the acceptor-TψC stem-loop domain of $SctRNA^{Phe}_{GAA}$. The dissociation profiles obtained for both $SctRNA^{Phe}_{GAA}$ and $minihelix^{Phe}$ were different at most by a factor of two (compare competitive EMSAs Figure 4B), confirming the low binding specificity of transcripts in general. In addition, transcripts were found to be poor ligands as they dissociate the tRip:$Sctr^{Phe}_{GAA}$ complex at levels only comparable to the low group of native *S. cerevisiae* tRNAs. Altogether, those observations hint that tRip does not focus on the tRNA's primary sequence, but rather relies at least partially on individual post-transcriptional modifications or sets of modifications to discriminate between individual species.

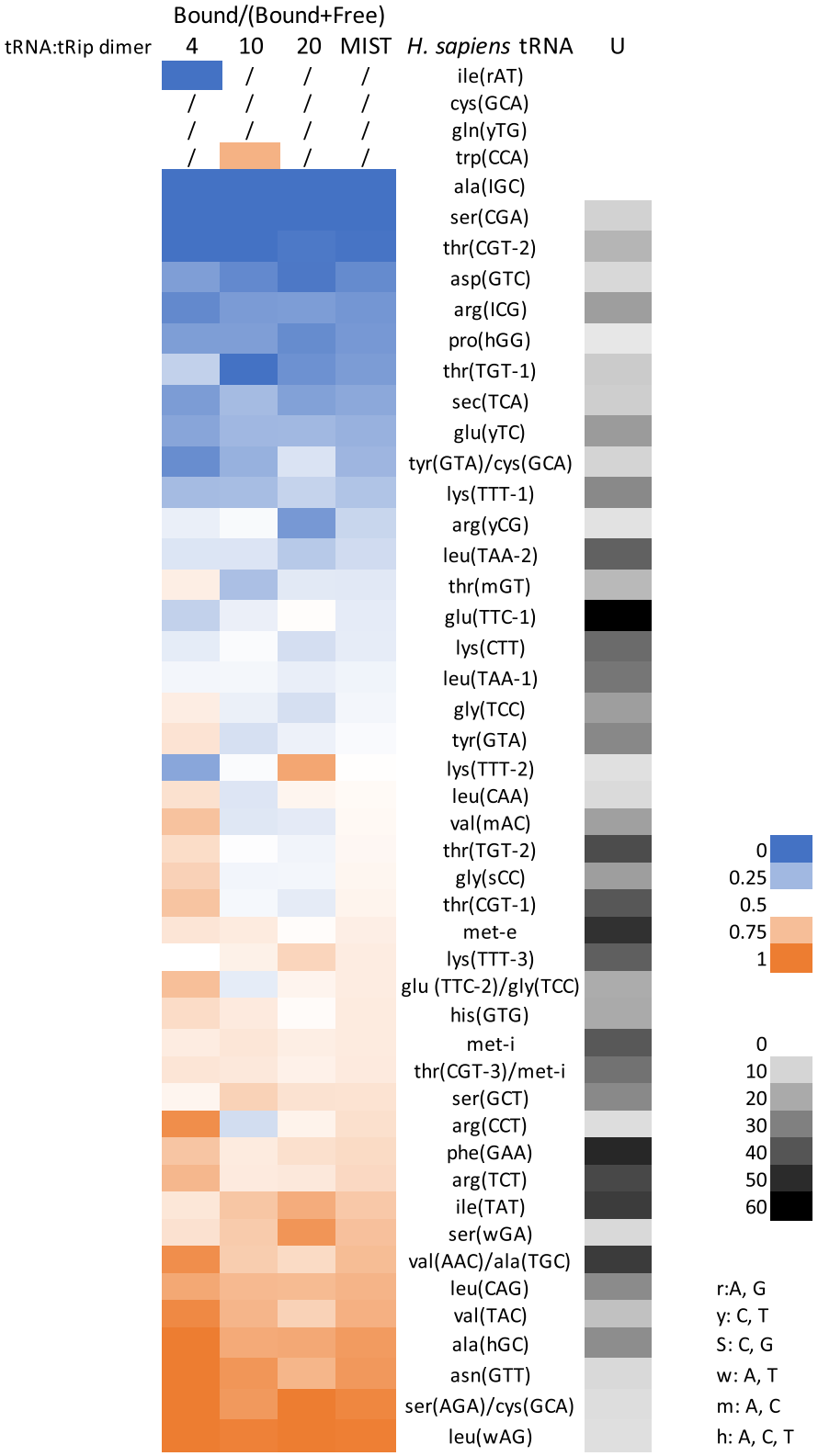

Figure 3. MIST results. The proportion of individual tRNAs present in two human crude tRNA samples (unselected tRNAs-1 and unselected tRNAs- 2) were measured, averaged, and displayed as shades of gray in the U column. The numbers 4, 10, 20 correspond to the fold excess of tRNA molecules relative to tRip dimers. The endpoint results are represented as bound tRNA/(bound + Free tRNA) for each tRNA:tRip dimer ratio. The average of the three MIST replicates was used to rank tRNAs according to their relative affinity for tRip. The orange color corresponds to the tRNAs most represented in the bound fraction and blue corresponds to the least represented tRNAs. Measurements below detection limit are marked with a slash (/). Some tRNAs bind to more than one probe (Supplementary Figure S1 and S3). For example, $tRNA^{Cys}_{GCA}$ hybridizes to probes Ser-4h and Tyr-1h. However, since Tyr-1h does yield a strong signal, we assumed that Ser-4h hybridizes mainly $tRNA^{Ser}_{AGA}$, which also happens to be one of the best tRip ligands.

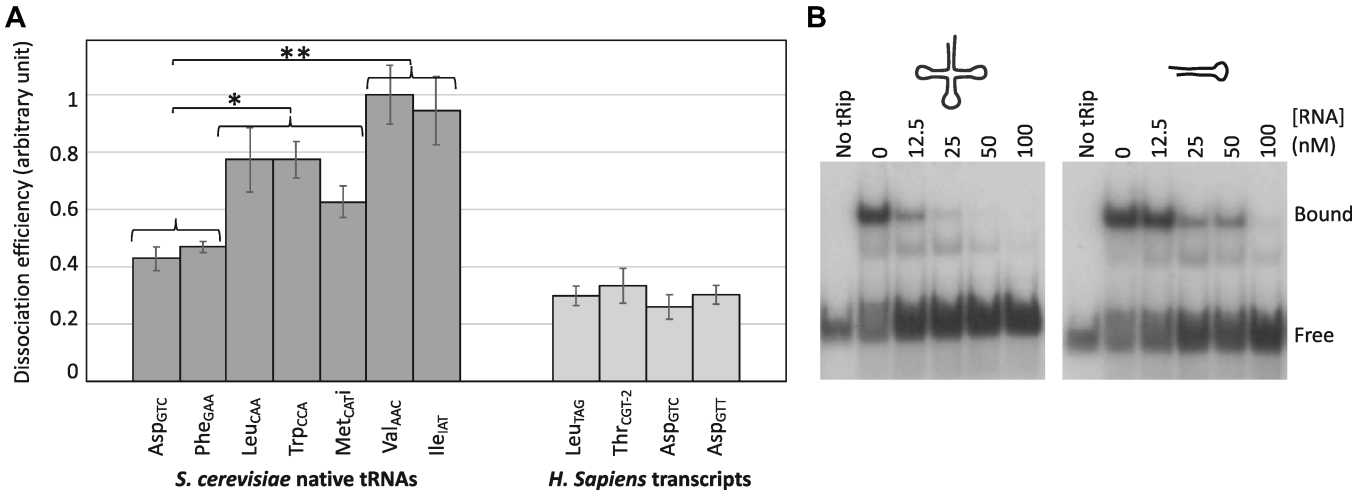

Figure 4. tRip does not recognize native and in vitro transcribed tRNAs in the same way. (**A**) Comparisons of dissociation rates obtained with *S. cerevisiae* tRNAs and *H. sapiens* transcripts. The bar graph represents the mean and SEM of at least three independent experiments, where dissociation rates of the Sctr$^{Phe}_{GAA}$:tRip complex were determined in the presence of increasing concentrations of seven *S. cerevisiae* native tRNAs (tRNA$^{Asp}_{GTC}$, tRNA$^{Phe}_{GAA}$, tRNA$^{Leu}_{CAA}$, tRNA$^{Trp}_{CCA}$, tRNA^{Met}i, tRNA$^{Val}_{AAC}$ and tRNA$^{Ile}_{IAT}$) and four different *H. sapiens* tRNA transcripts (tr$^{Thr}_{CGT-2}$, tr$^{Asp}_{GTC}$, tr$^{Leu}_{TAG}$ and tr$^{Asn}_{GTT}$). *P*-values were calculated (t-test) by comparing the dissociation rates two by two (**$P < 0.005$ and *$P < 0.01$). (**B**) Competitive EMSAs with *S. cerevisiae* tRNA$^{Phe}_{GAA}$ and minihelix^{Phe}. Competitive EMSAs performed under identical conditions challenged the formation of complexes between radiolabeled Sctr$^{Phe}_{GAA}$ and tRip (30 nM) with increasing concentrations (12.5, 25, 50 and 100 nM) of SctRNA$^{Phe}_{GAA}$ or minihelix^{Phe}, as indicated. The latter mimics the tRNA acceptor domain encompassing the acceptor stem and the T-domain. Samples were analyzed on native polyacrylamide gels. Gel images are representative of three biological replicates.

DISCUSSION

tRip is a 402-amino acid polypeptide highly conserved in *Plasmodia* (Figure 1A) involved in exogenous tRNA import. tRip is an integral membrane protein found in the plasma membrane, with its tRNA binding domain located at the parasite surface, where it presumably comes in contact with host tRNAs (4). As in *H. sapiens* AIMP1, the C-terminal domain of tRip consists of two domains that act in concert to efficiently bind tRNAs: the OB-fold domain with a few residues essential for recognition (Ser_{312} and Met_{315}), and a short linker region, which is rich in positively charged amino acids, and greatly increases the binding strength (Figure 1B). Like its bacterial homolog Trbp111, tRip recognizes and binds the corner formed by the D- and T- loops, a motif common to all tRNA 3D structures, which explains why this protein interacts with multiple different tRNAs (Figure 4B). According to our model, tRip also binds to the variable region and the upper part of the anticodon arm of tRNAs (Figure 1C).

This model of tRNA recognition solely based on the tRNA structure is challenged by two studies that showed that *S. cerevisiae* Arc1p and *T. brucei* MCP2 interact exclusively with a limited number of tRNAs (Supplementary Figure S4) (17,18). Using MIST, we also identified the species of human tRNAs that are preferentially recognized by tRip. *H. sapiens* tRNA$^{Ala}_{hGC}$, tRNA$^{Asn}_{GTT}$, tRNA$^{Ser}_{AGA}$ and tRNA$^{Leu}_{wAG}$ are highly enriched in the tRip-bound fraction, while tRNA$^{Ala}_{IGC}$, tRNA$^{Ser}_{CGA}$, tRNA$^{Thr}_{CGT-2}$, tRNA$^{Asp}_{GTC}$, tRNA$^{Arg}_{ICG}$ and tRNA$^{Pro}_{hGC}$ are clearly underrepresented (Figure 3). Sequence comparison of members of these two groups did not reveal any obvious motifs involved in tRip recognition. Furthermore, our experiments show that only native tRNAs are properly distinguished by tRip; whereas the corresponding unmodified transcripts form complexes with the enzyme indiscriminately (Figure 4A).

Apart from their primary sequence, tRNAs are characterized by the presence of numerous post-transcriptional modifications. Many modifications are located in the corner of the tRNA 3D structure, which is precisely the region protected by tRip in footprint experiments (Figure 1C and Supplementary Figure S2). In particular, these post-transcriptional modifications are important for proper tRNA folding and stability (reviewed in (37,38,39)). Therefore, we searched the Modomics database (40) with the tRNAs tested herein against all vertebrate cytosolic tRNAs harboring known post-transcriptional modifications. We obtained 19 matches with tRNA sequences representative of a wide range of relative affinities and catalogued the corresponding modifications located in their D-arm, D-loop, anticodon arm, variable region, and T-loop (Figure 5A). Among those modifications, some are absent amongst the weakest tRip-binders (tRNA$^{Asp}_{GTC}$, tRNA$^{Arg}_{iCG}$ and tRNA$^{Glu}_{yTC}$) such as N4-acetylcytidine (ac4C) at position 12 in the D-loop, one or several pseudouridine (Ψ) in the anticodon arm, or 7-methylguanosine (m7G) in the variable region. Thus, we can hypothesize that the presence of these modifications promotes recognition by tRip. Modification patterns such as Ψ at position 13 in the D-arm, two consecutive 5-methylcytidine (m5C) in the variable region, or 5,2′-*O*-dimethyluridine (m5Um) in the T-loop are absent amongst the strongest tRip-binders (tRNA$^{Arg}_{TCT}$, tRNA$^{Ser}_{wGA}$, tRNA^{Asn}GTT and tRNA$^{Leu}_{wAG}$). The presence of those modifications in other tRNAs could explain their impaired ability to form complexes with tRip. In other words, ac4C at position 12, Ψ in the anticodon arm, and

A

		D-arm			D-loop								Ac-arm-5'			Ac-arm-3'		Variable region				T-loop			species
M	tRNA	9	10	12	13	14	16	17	18	20	20a	20b	26	27	28	39	40	46	47	48	49	50	54	55	58	
0.1	Asp_{GTC}				Ψ					D										m5C	m5C		T	Ψ		*R. norvegicus GTC*
0.1	Arg_{iCG}	m1G	m2G				D				D		m2,2G						D		m5C	m5C			m1A	*H. sapiens* (this study)
0.2	Glu_{yTC}		m2G		Ψ					D	Ψ										m5C	m5C	m5Um	Ψ		*H.sapiens CTC*
0.4	Arg_{yCG}	m1G	m2G				D		Gm		D			Ψ					D			Ψ	T	Ψ	m1A	*B.taurus CCG*
0.4	$Glu_{TTC\text{-}1}$	m1G			Ψ					D	D										m5C	m5C	m5Um	Ψ		*R.norvegicuus TTC*
0.4	Lys_{CTT}		m2G				D			D				Ψ		Ψ		m7G	D	m5C	m5C		m5Um	Ψ	m1A	*R.norvegicuus CTT*
0.5	Tyr_{GTA}		m2G				(D)	D		acp3U			m2,2G	m2,2G		m1Ψ		m7G	D	m5C			T	Ψ	m1A	*H.sapiens GTA*
0.5	Leu_{CAA}		m2G	ac4C						D		Ψ	m2,2G			Ψ	Ψ			m5C	m5C		T	Ψ	m1A	*H.sapiens GAA*
0.5	Val_{mAC}				Ψ		D			D	D		m2G	Ψ				m7G	D	m5C	m5C			Ψ	m1A	*H.sapiens CAC*
0.5	Gly_{sCC}									D										m5C	m5C	m5C	T	Ψ	m1A	*H. sapiens GCC*
0.5	Gly_{sCC}				Ψ					D						Ψm					m5C	m5C	T	Ψ	m1A	*H. sapiens CCC*
0.6	Met_{CATe}		m2G				D			D			m2G	Ψ		Ψ		m7G	D	m5C			T	Ψ	m1A	*H.sapiens CTA*
0.6	His_{GTG}				Ψ		D			D	D									m5C	m5C			Ψ	m1A	*H.sapiens CTG*
0.6	Met_{CATi}	m1G	m2G										m2G					m7G	D	m5C					m1A	*H.sapiens ini*
0.6	Ser_{GCT}			ac4C			D		Gm	D	D		m2,2G		Ψ	Ψ				m5C			T	Ψ	m1A	*R.norvegicus GCT*
0.6	Phe_{GAA}		m2G			m1A	D	D					m2,2G	Ψ	Ψ	Ψ		m7G	D		m5C		T	Ψ	m1A	*H.sapiens GAA*
0.7	Arg_{TCT}	m1G									m1G			Ψ	Ψ			m7G	D		m5C					*B.taurus TCT*
0.7	Ser_{wGA}			ac4C			D		Gm	D	D				Ψ	Ψ				m5C			T	Ψ	m1A	*H.sapiens TGA*
0.9	Asn_{GTT}	m1G	m2G				D			D	acp3U		m2,2G	Ψ	Ψ			m7G	D				?	Ψ	m1A	*H.sapiens GTT*
1.0	Leu_{wAG}		m2G	ac4C						D	D		m2,2G							m5C			T	Ψ	m1A	*B.taurus IAG*

B

Figure 5. Possible involvement of post-transcriptional modifications in tRNA recognition by tRip. (**A**) Results from screening of the Modomics database (40) for modifications potentially involved in tRNA:tRip complex formation. Known post-transcriptional modifications are shown for human tRNAs or, when appropriate, for vertebrate tRNAs that are 100% identical to the corresponding human tRNA. The tRNAs are presented according to their relative affinity for tRip as determined by MIST. The tRNAs characterized by the lowest and the highest affinities are highlighted in blue and orange, respectively. Post-transcriptional modifications are highlighted in blue when they are always absent from tRNAs with the highest binding capacities and are thus potentially unfavorable for the interaction with tRip (negative or anti-determinants). Conversely, post-transcriptional modifications in orange are absent from tRNAs with the lowest binding capacities and are thus potentially supporting the interaction with tRip (positive determinants). Modifications are abbreviated as following: ac4C (N4-acetyl-2′-O-methylcytidine), acp3U (3-(3-amino-3-carboxypropyl)-5,6-dihydrouridine), Ψ (pseudouridine), m1Ψ (1-methylpseudouridine), Ψm (2′-O-methylpseudouridine), m1G (1-methylguanosine), m7G (7-methylguanosine), m2G (N2-methylguanosine), Gm (2′-*O*-methylguanosine), m2,2G (N2,N2-dimethylguanosine), m5C (5-methylcytidine), m5Um (5,2′-O-dimethyluridine), m1A (1-methyladenosine), T (5-methyluridine), D (dihydrouridine). (**B**) Spatial distribution of modifications potentially involved in tRNA:tRip complex formation. Modifications identified in (A) were placed on the crystallographic structure of *S. cerevisiae* $tRNA^{Phe}_{GAA}$ (pdb1EHZ) using the same color code. The tRNA structure in the middle recapitulates the regions of $Sctr^{Phe}_{GAA}$ that are in contact with tRip as determined by footprint experiments (Figure 1C and Supplementary Figure S2). Nucleotides strongly protected from Pb^{2+} cleavage are indicated in green and nucleotides moderately protected are in yellow.

m7G can be considered to be positive determinants for tRip complex formation and Ψ at position 13, two m5C modifications in the variable loop and m5Um in the T-loop can be considered as anti-determinants for tRip recognition. Interestingly, we observe a progressive blending of modifications that favor and disfavor complex formation in moderate tRip-binders (in beige). Finally, the tRNA 3D structure clearly shows that (i) the localization of these modifications coincides with nucleotides protected by the C-terminal domain of tRip and (ii) pro- and anti-complex modifications seem to segregate (Figure 5B). Although those observations are striking, they raise fundamental questions: Are those post-transcriptional modifications directly recognized by tRip or do they rather modulate the local structure of their tRNA? Do they act individually or in synergy? Further investigation will be necessary to shed additional light on the molecular mechanism that controls the formation of the tRNA:tRip complex, especially in understanding whether the base modifications are true binding sites or whether they contribute to the recognition of the mature tRNA folded structure.

The different tRNAs species in *Plasmodium* are all encoded by single-copy genes, a pattern that is rather unusual in eukaryotes (41). Although the number of copies of tRNA genes typically correlates poorly with cellular tRNA concentrations, one can wonder how an organism with such uniform tRNA gene organization supports the translation of widely distributed codons. Thus, for all human tRNAs tested with MIST herein, we looked at the codons they decode and their usage in the parasite genome. We hypothesized that species that bind strongly to tRip could be preferentially imported into the parasite where they could boost the translation of abundant codons in the parasite transcriptome ((42), Supplementary Table S2). As a whole, the data shown in Figure 6 does not support this hypothesis. However, it is worth noting that while *H. sapiens* $tRNA^{Asn}_{GTT}$ is among the strongest tRip ligands, asparagine (Asn) is also the predominant amino acid (along

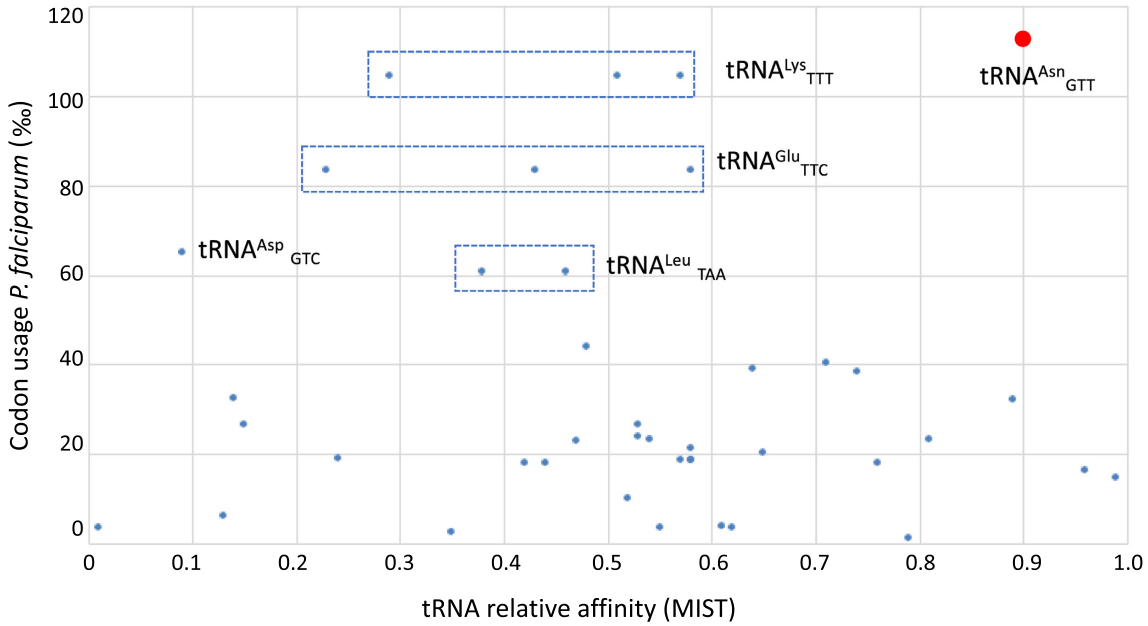

Figure 6. Differential affinities of human tRNAs for tRip *versus* codon usage in *P. falciparum*. Each dot corresponds to a tRNA defined by its affinity for tRip as determined by MIST (x-axis) and the frequency of the codons it could potentially translate assuming it participated in *P. falciparum* protein translation (y-axis, $^{0}/_{00}$) (42). The tRNAs corresponding to the amino acids used most frequently in translation by the parasite are indicated by dashed rectangles. $tRNA^{Asn}_{GTT}$, which is relevant for the translation of asparagine homorepeats that are abundant in *P. falciparum* proteins, is highlighted separately (red dot).

with lysine) in the *P. falciparum* proteome. Further, Asn is not homogeneously distributed in proteins as the majority of Asn is found in insertions of low complexity which often form long homopolymeric regions (43). Although Asn-rich insertions are present in all *Plasmodium* proteins except in ribosomal proteins, their role is still much debated. In their recent review, Davies and collaborators summarize the many processes in which these repeats are suspected to be involved, such as protein-protein interactions and/or aggregation, protein localization, immune response, or parasite virulence (44). Additionally, our team has previously hypothesized that Asn homorepeats could directly slow down translating ribosomes and therefore favor proper cotranslational folding of *Plasmodium* proteins (45).

In another *in vitro* study, we showed that the cytosolic *P. falciparum* asparaginyl-tRNA synthetase aminoacylates human $tRNA^{Asn}$ transcripts with an 8-fold reduced catalytic efficiency compared to *P. falciparum* $tRNA^{Asn}$ transcripts (46). Although this observation seems to be at odds with the possible involvement of host $tRNA^{Asn}$ in parasite protein translation, it is crucial to remember that the substrates used in the corresponding work entirely lacked post-transcriptional modifications that are known to play a significant role in the folding and aminoacylation of tRNAs (37). Specifically, human $tRNA^{Asn}_{GTT}$ displays two prominent modifications at positions 34 and 37 in the anticodon loop (a queuosine and an N6-threonylcarbamoyladenosine, respectively), which are potentially recognized as identity elements supporting aminoacylation.

To date, *Plasmodium* tRip is the only known protein supporting the intracellular import of exogenous tRNAs. As such it might represent a novel pathway that supports host-parasite interactions and sustains infection. In this context, complementing the pool of tRNAs transcribed by the parasite with the import of specific exogenous/host tRNAs could play a punctual role during the developmental cycle, either by promoting protein synthesis at specific stages or by enabling unrelated signaling processes such as those reviewed in (47,48,49). The absence of other examples of import of exogenous tRNAs beyond the *Plasmodium* genus complicates its characterization but also offers new opportunities. Orphan proteins, such as tRip, require creative bottom-up investigative approaches. However, their singularity also offers the potential for the development of pioneering antimalarial treatments.

DATA AVAILABILITY

Array data files can be found at Gene Expression Omnibus GSE179567.

SUPPLEMENTARY DATA

Supplementary Data are available at NAR Online.

ACKNOWLEDGEMENTS

We are grateful to Laura Antoine, Annika Breidenstein and Caroline Paulus for their technical assistance as well as Ansley Elkins and Professor Tamara Hendrickson for providing comments on this manuscript.

FUNDING

Interdisciplinary Thematic Institute IMCBio, as part of the ITI 2021–2028 program of the University of Strasbourg, CNRS and Inserm; IdEx Unistra [ANR-10-IDEX-0002]; SFRI-STRAT'US project [ANR 20-SFRI-0012]; EUR IMCBio [IMCBio ANR-17-EURE-0023] under the framework of the French Investments for the Future Program ≫; Labex NetRNA [ANR-10-LABX-0036]; CNRS and the Université de Strasbourg to Magali Frugier and the Fondation pour la Recherche Médicale (FRM) [FDT201704337050 to M.C.]; SC INBRE grant from the National Institute of General Medical Science – NIH [P20GM103499 to R.G.]. Funding for open access charge: ANR-10-LABX-0036_NETRNA.

Conflict of interest statement. None declared.

REFERENCES

1. World Health Organization (2019) World malaria report 2019.
2. Cowman,A.F., Healer,J., Marapana,D. and Marsh,K. (2016) Malaria: biology and disease. *Cell*, **167**, 610–624.
3. Sato,S. (2021) Plasmodium-a brief introduction to the parasites causing human malaria and their basic biology. *J. Physiol. Anthropol.*, **40**, 251–259.
4. Bour,T., Mahmoudi,N., Kapps,D., Thiberge,S., Bargieri,D., Ménard,R. and Frugier,M. (2016) *Apicomplexa* -specific tRip facilitates import of exogenous tRNAs into malaria parasites. *Proc. Natl Acad. Sci. U.S.A.*, **113**, 4717–4722.
5. Ibba,M. and Soll,D. (2000) Aminoacyl-tRNA synthesis. *Annu. Rev. Biochem.*, **69**, 617–650.
6. Morales,A.J., Swairjo,M.A. and Schimmel,P. (1999) Structure-specific tRNA-binding protein from the extreme thermophile Aquifex aeolicus. *EMBO J.*, **18**, 3475–3483.
7. Swairjo,M.A., Morales,A.J., Wang,C.C., Ortiz,A.R. and Schimmel,P. (2000) Crystal structure of Trbp111: a structure-specific tRNA-binding protein. *EMBO J.*, **19**, 6287–6298.
8. Simos,G., Sauer,A., Fasiolo,F. and Hurt,E.C. (1998) A conserved domain within Arc1p delivers tRNA to Aminoacyl-tRNA synthetases. *Mol. Cell*, **1**, 235–242.
9. Kapps,D., Cela,M., Théobald-Dietrich,A., Hendrickson,T. and Frugier,M. (2016) OB or Not OB: idiosyncratic utilization of the tRNA-binding OB-fold domain in unicellular, pathogenic eukaryotes. *FEBS Lett.*, **590**, 4180–4191.
10. Renault,L., Kerjan,P., Pasqualato,S., Ménétrey,J., Robinson,J.-C., Kawaguchi,S., Vassylyev,D.G., Yokoyama,S., Mirande,M. and Cherfils,J. (2001) Structure of the EMAPII domain of human aminoacyl-tRNA synthetase complex reveals evolutionary dimer mimicry. *EMBO J.*, **20**, 570–578.
11. Shalak,V., Kaminska,M., Mitnacht-Kraus,R., Vandenabeele,P., Clauss,M. and Mirande,M. (2001) The EMAPII cytokine is released from the mammalian multisynthetase complex after cleavage of its p43/proEMAPII component. *J. Biol. Chem.*, **276**, 23769–23776.
12. Golinelli-Cohen,M.-P. and Mirande,M. (2007) Arc1p is required for cytoplasmic confinement of synthetases and tRNA. *Mol. Cell. Biochem.*, **300**, 47–59.
13. Negrutskii,B.S. and Deutscher,M.P. (1991) Channeling of aminoacyl-tRNA for protein synthesis in vivo. *Proc. Natl. Acad. Sci.*, **88**, 4991–4995.
14. Quevillon,S., Agou,F., Robinson,J.-C. and Mirande,M. (1997) The p43 component of the mammalian Multi-synthetase complex is likely to be the precursor of the endothelial monocyte-activating polypeptide II cytokine. *J. Biol. Chem.*, **272**, 32573–32579.
15. Wakasugi,K. and Schimmel,P. (1999) Two distinct cytokines released from a human aminoacyl-tRNA synthetase. *Science*, **284**, 147–151.
16. Zhou,Z., Sun,B., Huang,S., Yu,D. and Zhang,X. (2020) Roles of aminoacyl-tRNA synthetase-interacting multi-functional proteins in physiology and cancer. *Cell Death. Dis.*, **11**, 579.
17. Cestari,I., Kalidas,S., Monnerat,S., Anupama,A., Phillips,M.A. and Stuart,K. (2013) A multiple aminoacyl-tRNA synthetase complex that enhances tRNA-aminoacylation in african trypanosomes. *Mol. Cell. Biol.*, **33**, 4872–4888.
18. Deinert,K., Fasiolo,F., Hurt,E.C. and Simos,G. (2001) Arc1p organizes the yeast aminoacyl-tRNA synthetase complex and stabilizes its interaction with the cognate tRNAs. *J. Biol. Chem.*, **276**, 6000–6008.
19. Simader,H., Hothorn,M., Köhler,C., Basquin,J., Simos,G. and Suck,D. (2006) Structural basis of yeast aminoacyl-tRNA synthetase complex formation revealed by crystal structures of two binary sub-complexes. *Nucleic Acids Res.*, **34**, 3968–3979.
20. Frechin,M., Enkler,L., Tetaud,E., Laporte,D., Senger,B., Blancard,C., Hammann,P., Bader,G., Clauder-Münster,S., Steinmetz,L.M. *et al.* (2014) Expression of nuclear and mitochondrial genes encoding ATP synthase is synchronized by disassembly of a multisynthetase complex. *Mol. Cell.*, **56**, 763–776.
21. Galani,K., Großhans,H., Deinert,K., Hurt,E.C. and Simos,G. (2001) The intracellular location of two aminoacyl-tRNA synthetases depends on complex formation with Arc1p. *EMBO J.*, **20**, 6889–6898.
22. Simos,G., Segref,A., Fasiolo,F., Hellmuth,K., Shevchenko,A., Mann,M. and Hurt,E.C. (1996) The yeast protein Arc1p binds to tRNA and functions as a cofactor for the methionyl- and glutamyl-tRNA synthetases. *EMBO J.*, **15**, 5437–5448.
23. Eriani,G., Karam,J., Jacinto,J., Morris Richard,E. and Geslain,R. (2015) MIST, a novel approach to reveal hidden substrate specificity in aminoacyl-tRNA synthetases. *PLoS One*, **10**, e0130042.
24. Yokogawa,T., Kitamura,Y., Nakamura,D., Ohno,S. and Nishikawa,K. (2010) Optimization of the hybridization-based method for purification of thermostable tRNAs in the presence of tetraalkylammonium salts. *Nucleic Acids Res.*, **38**, e89.
25. Giegé,R., Dock,A.C., Kern,D., Lorber,B., Thierry,J.C. and Moras,D. (1986) The role of purification in the crystallization of proteins and nucleic acids. *J. Cryst. Growth*, **76**, 554–561.
26. Heitzler,J., Maréchal-Drouard,L., Dirheimer,G. and Keith,G. (1992) Use of a dot blot hybridization method for identification of pure tRNA species on different membranes. *Biochim. Biophys. Acta (BBA) - Gene Struct. Express.*, **1129**, 273–277.
27. Antoine,L. and Wolff,P. (2020) Mapping of posttranscriptional tRNA modifications by Two-Dimensional gel electrophoresis mass spectrometry. In: Arluison,V. and Wien,F. (eds). *RNA Spectroscopy Methods in Molecular Biology*. Springer, NY, pp. 101–110.
28. Vlassov,V.V., Giegé,R. and Ebel,J.P. (1980) The tertiary structure of yeast tRNA ^{Phe} in solution studied by phosphodiester bond modification with ethylnitrosourea. *FEBS Lett.*, **120**, 12–16.
29. Silberklang,M., Gillum,A.M. and Rajbhandary,U.L. (1977) The use of nuclease P_1 in sequence analysis of end group labeled RNA. *Nucl Acids Res*, **4**, 4091–4108.
30. Schatz,D., Leberman,R. and Eckstein,F. (1991) Interaction of Escherichia coli tRNA(Ser) with its cognate aminoacyl-tRNA synthetase as determined by footprinting with phosphorothioate-containing tRNA transcripts. *Proc. Natl. Acad. Sci. U.S.A.*, **88**, 6132–6136.
31. Petrov,A., Wu,T., Puglisi,E.V. and Puglisi,J.D. (2013) RNA purification by preparative polyacrylamide gel electrophoresis. In: *Methods in Enzymology*. Elsevier, pp. 315–330.
32. Emetu,S., Troiano,M., Goldmintz,J., Tomberlin,J., Grelet,S., Howe,P.H., Korey,C. and Geslain,R. (2018) Metabolic labeling and profiling of transfer RNAsusing macroarrays. *JoVE*, **131**, 56898.
33. Lindell,M., Romby,P. and Wagner,E.G.H. (2002) Lead(II) as a probe for investigating RNA structure in vivo. *RNA*, **8**, 534–541.
34. Nomanbhoy,T., Morales,A.J., Abraham,A.T., Vörtler,C.S., Giegé,R. and Schimmel,P. (2001) Simultaneous binding of two proteins to opposite sides of a single transfer RNA. *Nat. Struct. Biol.*, **8**, 344–348.
35. Gupta,S., Chhibber-Goel,J., Sharma,M., Parvez,S., Harlos,K., Sharma,A. and Yogavel,M. (2020) Crystal structures of the two domains that constitute the Plasmodium vivax p43 protein. *Acta Crystallogr. D Struct. Biol.*, **76**, 135–146.
36. Dittmar,K.A., Goodenbour,J.M. and Pan,T. (2006) Tissue-Specific differences in human transfer RNA expression. *PLoS Genet.*, **2**, e221.
37. Giegé,R. (2008) Toward a more complete view of tRNA biology. *Nat. Struct. Mol. Biol.*, **15**, 1007–1014.
38. Hopper,A.K. (2013) Transfer RNA Post-transcriptional processing, turnover, and subcellular dynamics in the yeast *Saccharomyces cerevisiae*. *Genetics*, **194**, 43–67.

39. Motorin,Y. and Helm,M. (2010) tRNA stabilization by modified nucleotides. *Biochemistry*, **49**, 4934–4944.
40. Boccaletto,P., Machnicka,M.A., Purta,E., Piątkowski,P., Bagiński,B., Wirecki,T.K., de Crécy-Lagard,V., Ross,R., Limbach,P.A., Kotter,A. *et al.* (2017) MODOMICS: a database of RNA modification pathways. *Nucleic Acids Res.*, gkx1030.
41. Gardner,M.J., Hall,N., Fung,E., White,O., Berriman,M., Hyman,R.W., Carlton,J.M., Pain,A., Nelson,K.E., Bowman,S. *et al.* (2002) Genome sequence of the human malaria parasite *Plasmodium falciparum*. *Nature*, **419**, 498–511.
42. Nakamura,Y. (2000) Codon usage tabulated from international DNA sequence databases: status for the year 2000. *Nucleic Acids Res.*, **28**, 292–292.
43. Chaudhry,S.R., Lwin,N., Phelan,D., Escalante,A.A. and Battistuzzi,F.U. (2018) Comparative analysis of low complexity regions in Plasmodia. *Sci. Rep.*, **8**, 335.
44. Davies,H.M., Nofal,S.D., McLaughlin,E.J. and Osborne,A.R. (2017) Repetitive sequences in malaria parasite proteins. *FEMS Microbiol. Rev.*, **41**, 923–940.
45. Frugier,M., Bour,T., Ayach,M., Santos,M.A., Rudinger-Thirion,J., Théobald-Dietrich,A. and Pizzi,E. (2010) Low Complexity Regions behave as tRNA sponges to help co-translational folding of plasmodial proteins. *FEBS Lett.*, **584**, 448–454.
46. Filisetti,D., Théobald-Dietrich,A., Mahmoudi,N., Rudinger-Thirion,J., Candolfi,E. and Frugier,M. (2013) Aminoacylation of Plasmodium falciparum tRNAAsn and insights in the synthesis of asparagine repeats. *J. Biol. Chem.*, **288**, 36361–36371.
47. Krishna,S., Raghavan,S., DasGupta,R. and Palakodeti,D. (2021) tRNA-derived fragments (tRFs): establishing their turf in post-transcriptional gene regulation. *Cell. Mol. Life Sci.*, **78**, 2607–2619.
48. Schimmel,P. (2018) The emerging complexity of the tRNA world: mammalian tRNAs beyond protein synthesis. *Nat. Rev. Mol. Cell Biol.*, **19**, 45–58.
49. Shikha,S., Brogli,R., Schneider,A. and Polacek,N. (2019) tRNA biology in trypanosomes. *Chimia*, **73**, 395–405.
50. Warrenfeltz,S., Basenko,E.Y., Crouch,K., Harb,O.S., Kissinger,J.C., Roos,D.S., Shanmugasundram,A. and Silva-Franco,F. (2018) EuPathDB: the eukaryotic pathogen genomics database resource. *Methods Mol. Biol.*, **1757**, 69–113.